Quantifying Uplift using Decompaction: A case study from the Exmouth Plateau, North West Shelf

Patrick Makuluni
Minerals and Energy Resources
UNSW Sydney
Kensington, NSW
p.makuluni@unsw.edu.au

Laurent Langhi
Energy Resources
CSIRO
Kensington, WA
laurent.langhi@csiro.au

Juerg Hauser
Mineral Resources
CSIRO
Kensington, WA
juerg.hauser@csiro.au

Stuart Clark
Mineral and Energy Resources
UNSW Sydney
*Kensington, NSW*
stuart.clark@unsw.edu.au

SUMMARY

Uplift events have caused the failure of hydrocarbon seals resulting from subsequent deformation and fault development or reactivation. On the other hand, escaping hydrocarbons from the breached seals may accumulate in new traps, and fracturing of brittle reservoir rocks during uplift enhances reservoir productivity. These and other factors justify the importance of quantifying and constraining the distribution of uplift within sedimentary basins for hydrocarbon exploration purposes. Multiple studies have discovered evidence of uplift in the Exmouth Plateau of the Northern Carnarvon Basin; however, the temporal and spatial distribution of this uplift has not been fully quantified. Common methods use sediments' thermal properties to estimate maximum burial depth and subsequently quantify and constrain sediment uplift. However, these thermal-based methods lack accuracy where sediments have been heated by magmatic intrusions, for example, the Triassic Mungaroo formation sediments in the Northern Carnarvon Basin. In this work, we use compaction-derived methods to quantify and constrain the distribution of uplift and its impact on the hydrocarbon systems in the Exmouth Plateau, Northern Carnarvon Basin. We used porosity data (corrected for digenesis) from 68 wells of the Australian National Offshore Petroleum Information Management System (NOPIMS) to accurately estimate maximum burial depths and subsequently estimate uplift. Results indicate larger uplift (up to 1.4km) in the central and southwestern part of the Exmouth Plateau from mid-Triassic to the present. The spatial distribution of uplift correlates with the distribution of magmatic intrusions in the region. We suggest that, in addition to compression, the multiple Late Triassic to Early Cretaceous rifting events in the Northern Carnarvon Basin triggered magmatic intrusions that produced permanent uplift. Uplift results from Vitrinite Reflectance are slightly higher than those from compaction-based methods, suggesting extra heat input from these intrusions. This uplift majorly controlled the distribution of Jurassic source rocks in the Northern Carnarvon Basin.

Keywords: Uplift, Exmouth Plateau, Porosity, magmatic intrusions, Hydrocarbon systems

INTRODUCTION

The Exmouth Plateau is a subsided continental platform that sits on the west of the Jurassic sub-basins of the Northern Carnarvon Basin (Fig. 1) in the Australian North West Shelf. The Northern Carnarvon Basin (NCB) went through four major rifting events: the late Carboniferous to early Permian rifting (Heine and

Müller, 2005), the Late Triassic rifting leading to the break-up between the Indian and Australian Plates (Metcalfe, 2013), Callovian extension, and Tithonian Extension (Gibbons et al., 2012; Heine and Müller, 2005). The earlier extension events created accommodation space and supplied sediments into the Exmouth Plateau region, while the later events starved the Exmouth Plateau of sediment supply (Longley et al., 2002). The thick (up to 8km) fluvial sandstones, siltstones, claystones, and shales of the Triassic Mungaroo Formation make up more than 60% of the Exmouth Plateau Stratigraphy. These Triassic sediments are overlain by thin Jurassic source rocks, Cretaceous clastics, and Cenozoic carbonates.
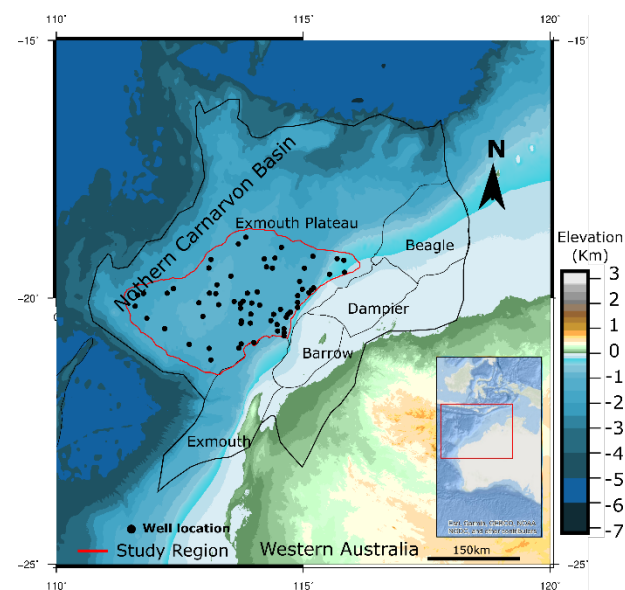
Figure 1: The study region (red) within the Exmouth Plateau plotted on a topographic map of the Northern Carnarvon Basin (NOAA NGDC, 2009), and showing the distribution of 68 wells (from NOPIMS) used in the uplift model. Figure produced using GMT (Wessel et al.,2019)

There are three significant sedimentation hiatuses between the Lower Jurassic and the Earliest Cretaceous period in the Exmouth Plateau stratigraphy (Fig. 2, Appendix). These hiatuses may be attributed to uplift and erosion or just a lack of sediment supply. Several studies (e.g., Longley et al., 2002; Paumard et al., 2018; Tindale et al., 1998) suggest that the Latest Triassic to Early Cretaceous rifting events tilted and uplifted fault blocks in the Northern Carnarvon Basin, as observed within the Exmouth Plateau. This uplift was followed by erosion and no sediment supply. Rohead-O'Brien and Elders (2018) constrained

the timing of uplift and erosion of these fault blocks in Exmouth Plateau. Their work suggests that fault block erosion started within the north-eastern Exmouth Plateau region in Rhaetian, then moved towards the center in the Latest Triassic to Early Jurassic. This erosion shifted towards the southwestern and central-western Exmouth Plateau in the Late Jurassic to the earliest Cretaceous period. The study of Rohrman (2015) proposed that a Late Jurassic mantle plume caused tectonic uplift and erosion in the southwestern parts of the Exmouth Plateau. Previously, Vera (1992) estimated up to 3.5km of erosion along the southwestern margin of this Exmouth Plateau region. They suggested that heat from the new oceanic ridge emplaced within this margin caused thermal uplift and erosion. The spatial and temporal distribution of such uplift and erosion may have impacted the development of petroleum systems in the Exmouth Plateau. This study aims at quantifying the temporal and spatial distribution of the uplift and its impacts on petroleum systems of the Exmouth Plateau. We combine compaction and thermal (vitrinite reflectance) methods to quantify uplift within boreholes then interpolate the results over the study region (Fig. 1) using GMT surface algorithms (Wessel et al., 2013).

METHOD AND RESULTS

Compaction Method

The porosity and density of sedimentary layers change with an increase in compaction and depth of burial (e.g., Allen and Allen, 2013; Athy, 1930; Magara, 1980). Sediment compaction is irreversible. Thus, when sedimentary layers are buried and compacted at a certain depth, their porosity or density remains constant even after being uplifted to a shallower depth. We apply this method to normally pressured sediments because mechanisms like overpressure, early oil charge, grain coating can interfere with the porosity depth relationship (Wilkinson et al., 2014; Wilkinson & Haszeldine, 2011). Hydrothermal processes like mineral dissolution and cementation can increase and reduce porosity, respectively (Allen and Allen, 2013). Sometimes the increment and reduction of porosity from these processes may cancel out or lessen their final impact (Lü et al., 2015; Surdam et al., 1984). Therefore, the final porosity (or density) data represent the maximum burial depth of normally pressured sediments. Athy (1930) developed this porosity depth relationship (Eq. 1) which suggests that the porosity of normally pressured sediments changes exponentially with an increase in depth. In equation 1: Φ_0 =initial porosity; Φ =measured porosity; c = exponential decay constant. Uplifted sediments, therefore, will plot above the normal porosity-depth curve, and the difference between the current depth and their maximum depth of burial (Eq.2) represents uplift. The maximum depth is calculated using equation 2, where X_{max}= maximum depth. This principle has been extensively used to estimate uplift in several regions: however, researchers use the sonic logs, which are readily available, unlike porosity data (Johnson et al., 2017; Magara, 1980; Poelchau, 1993; Tassone et al., 2014).

This work employs sandstone porosity data of the Triassic Mungaroo Formation (Fig.2 Appendix) from 68 wells (Fig. 1)

and eight shale sonic log data (e.g., Fig. 3, Appendix) from the National Offshore Petroleum Information Management Systems (NOPIMS) to estimate the amount of uplift in the southern Exmouth Plateau (Fig. 1). The initial porosity and porosity decay constants (Eq. 1) are extracted from literature (Allen and Allen, 2013; Sclater and Christie, 1980), while the porosity and depth information is extracted from NOPIMS (Table 1, Appendix). To estimate uplift using the sonic logs: the sonic interval transit time (from NOPIMS) is plotted against depth on the standard burial curve (Fig. 4, Johnson et al., 2017; Magara, 1980; Poelchau, 1993). The vertical displacement of the sample from the standard burial curve represents uplift. We constrain the timing of uplift using sedimentary age data from well-completion reports.

$$\Phi = \Phi_0 e^{-cy} \qquad (1)$$

$$X_{max} = \ln\left(\frac{\Phi}{\Phi_0}\right)\left(-\frac{1}{c}\right) \qquad (2)$$

Overall, the procedure involves modelling maximum burial depth using the porosity depth equations (1 & 2) and standard burial curve (Fig.3). We calculate uplift by subtracting the current sample depth from the calculated maximum depth while assuming mechanical compaction.

Thermal Method: Vitrinite Reflectance

Despite having some uncertainties in geologically complex regions with multiple heat sources, thermal methods still present significant evidence of uplift. Unlike the compaction methods, thermal methods use sediment temperature history to predict the maximum depth of burial (Bray et al., 1992; Duddy et al., 2004). These methods assume that temperature increase is caused by heat from burial, for example, Vitrinite Reflectance (VR) and Apatite Fission Track Analysis (AFTA) (Bray et al., 1992). Here we use the VR method. Vitrinite Reflectance is measured as a percentage reflectance in oil immersion and used to model sediments' maximum paleotemperature (Eq. 3). The paleotemperature is then applied to measure the thermal maturity of hydrocarbon source rocks (Barker & Pawlewicz, 1994; Bray et al., 1992; Burnham, 2019). In Eq. 3, T_{peak} =Maximum paleotemperature, R_0 =Vitrinite Reflectance. Vitrinite Reflectance data is presented in Table 2 (appendix).

$$T_{peak} = (\ln(R_0) + 1.68)/0.0124 \qquad (3)$$

This method involves two main steps. Firstly, we calculate maximum paleotemperature using the sample VR values (Eq.3). We then plot current temperature and maximum temperature against depth for every borehole and estimate paleo-geothermal gradients. Uplift is then calculated as the difference between the current temperature and maximum paleotemperature divided by the paleo-geothermal gradient (Eq. 4).

$$U = \left(T_{peak} - T_{current}\right)/\left(\frac{dT}{dz}\right)_{paleo} \qquad (4)$$

Thus, uplift is the difference between the sample depth and the maximum modelled paleo-depth. We then compare uplift results from vitrinite reflectance to those from compaction methods. We will also discuss any correlations between uplift and distribution of petroleum systems in the Exmouth Plateau. Finally, the study

will assess the current and paleo-geothermal gradients from the VR samples to predict the source of sediment heat using the models by Bray et al. (1992).

Results and Discussion

Fig. 5 shows the spatial distribution of uplift from the Triassic to the present. These estimates of uplift are from the compaction method and the porosity data. We created the map using a GMT surface algorithm (Wessel et al., 2013, 2019) which interpolates the results from all the sixty-eight wells (Fig. 1). The region went through an average of 1km uplift and a maximum of 1.4km uplift from the Late Triassic to the present. Assessing the shale sonic log data (Fig. 3) also suggests similar results to those from the porosity data. The highest uplift occurred in the southern and southwestern parts of the Exmouth Plateau, while the lowest uplift, of about 600m, occurred in the north and north-western parts of the Exmouth Plateau. There was limited porosity data from the younger sediments: however, results from the vitrinite reflectance method suggest that there has not been much uplift in the later stages of the geological evolution of the Exmouth Plateau (Fig. 6). Thus, Fig. 6 presents vitrinite reflectance plotted against depth for Jupiter 1 and Sirius 1 boreholes. The modelled paleo-geothermal gradient and the current geothermal gradient appear to be converging towards the top, and we observe a similar trend in all the other two wells (Vinck 1 and Saturn 1).

Petroleum systems in the NCB are classified into the Pre and Post Callovian-unconformity (Bishop, 1999). The Callovian unconformity refers to the regional erosional event that was caused by continental rifting, regional uplift, seafloor spreading, and prolonged sea-level lowstand within the Northwest Shelf (Longley et al., 2002). The Triassic Locker shale is the main source rock of the 'older' petroleum system, with the Triassic Mungaroo and Cretaceous Barrow Group reservoirs. Economic occurrences of this system are within the sub-basins, the eastern edge of Exmouth Plateau, and the Rankin Platform (Bishop, 1999). Hydrocarbon migration/escape is suspected to be the cause of non-economic occurrences towards the western part of the Exmouth Plateau region, where uplift (Fig. 5) created fluid pathways and reactivated pre-existing faults (Ruge et al., 2021; Velayatham et al., 2018). The main source rock for the 'younger' post-Callovian petroleum system is the Jurassic Dingo claystone, whose deposition was constrained within the Jurassic sub-basins and Rankin Platform, with minor accumulations within the Exmouth Plateau (Bishop, 1999; Longley et al., 2002). Studies further indicate that the Dingo Claystone in the Exmouth Plateau is not mature due to having a thin overburden, potentially caused by the Jurassic uplift and the subsequently reduced sediment supply (Bishop, 1999). Overall, the Jurassic uplift and erosion breached Triassic sediments in the Exmouth Plateau, potentially causing migration and escape of hydrocarbons from the 'older' Permo-Triassic petroleum system. This uplift and subsequent erosion starved the Exmouth Plateau of the Jurassic Dingo Claystone source rock, whose deposition was constrained within the eastern sub-basins. Reduced sediment supply slowed down the maturation of thin sections of the Dingo source rock in the Exmouth Plateau.
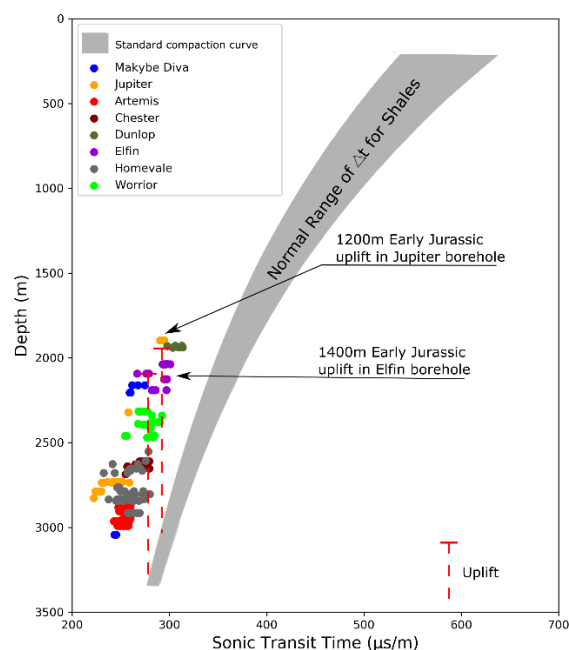
Figure 4: Results of uplift estimation using the shale standard burial curve, modified from (Poelchau, 1993). Six shale samples from Exmouth Plateau plot on the left of the normal shale compaction curve (grey area) signifying uplift.

The change (increase) in paleo-geothermal gradient with depth signifies sediment heating by an increased paleo-basal heat flow (Bray et al., 1992). This situation is common in regions with magmatic intrusions where the magmatic bodies supply extra heat to the sediments from the bottom. Table 2 presents a comparison of uplift results from the compaction and vitrinite reflectance methods. Table 2 indicates that the vitrinite reflectance method gives higher values of uplift compared to the compaction method. Thus, the VR method gives uplift values that are approximately 200 meters higher than those from the compaction method. There is good evidence of igneous intrusions in the Northern Carnarvon Basin, which are within the central part of Exmouth Plateau and most parts of the Exmouth Sub-basin in the southeastern part of the Northern Carnarvon Basin (Curtis et al., 2019; Holford and Schofield, 2013; McClay et al., 2013). The location of these magmatic intrusions (Fig. 7, Appendix) has a high spatial correlation with the highest uplift within the Exmouth Plateau (Fig. 1). From this correlation, we suggest that magmatic intrusions within the Exmouth Plateau may have contributed to the total observed uplift through a process of crustal underplating (Saunders et al., 2007; White and McKenzie, 1989). Regional magmatism (Curtis et al., 2019), which is likely responsible for the uplift (Brodie and White 1994), would have influenced the paleo-geotherm to be hotter than the present-day values from the well. This phenomenon would cause an overestimation in the uplift from VR. Such errors would not be present in the compaction method, which in this case, is likely to be a more accurate measure of the actual uplift experienced.
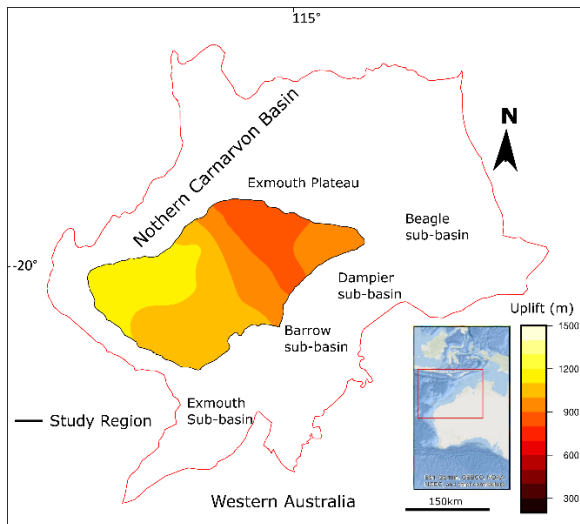
Figure 5: (top) Distribution of Uplift from compaction method. The southwestern part has higher uplift than the rest of the region. Figure produced using GMT (Wessel et al.,2019)
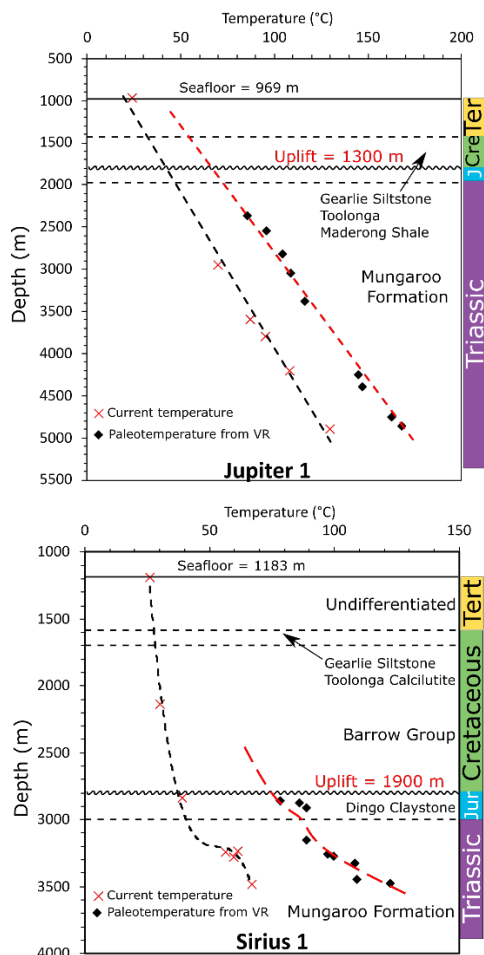

Figure 6: An example of vitrinite reflectance (VR) plotted against depth in Jupiter Well from the Exmouth Plateau. Black line = current temperature against depth, the red line = Paleotemperature against depth. Similar trends observed in Vinck1 and Saturn 1 boreholes.

Table 2: Comparing uplift results from thermal and compaction methods observed in four wells of the Exmouth Plateau. Uplift values from VR are slightly higher than those from compaction methods.

Well	Period	Uplift (m)	
		VR	Compaction
Sirius			
Latitude -20.8833	Post Jurassic	900	n/a
Longitude 112.6906	Post Triassic	1240	1020
Vinck			
Latitude -20.5834 Longitude 112.1939	Post Triassic	1300	990
Saturn			
Latitude -19.9086 Longitude 114.946	Post Jurassic	600	480
	Post Triassic	1230	1220
Jupiter			
Latitude -19.5802 Longitude 113.5342	Post Triassic	1450	1270

CONCLUSIONS

Approximately 1km of sediments have been uplifted and eroded from the Exmouth plateau region since the late Triassic to the present, with maximum values of approximately 1.4km within the southwestern part of the region. The vitrinite reflectance method gives comparatively higher uplift values since the Late Triassic but shows that the Exmouth Plateau went through minimal uplift since Jurassic. The spatial correlation between uplift and magmatic intrusions suggests that uplift was partly due to magmatic underplating, where heat from the intrusions caused vitrinite samples to record higher paleotemperatures than normal burial temperatures. Overall, the Jurassic uplift and erosion breached Triassic sediments in the Exmouth Plateau, potentially causing migration and escape of hydrocarbons from the Permo-Triassic petroleum systems. This uplift and subsequent erosion starved the Exmouth Plateau of the Jurassic source rock and slowed down its maturation in the Exmouth Plateau.

ACKNOWLEDGMENTS

REFERENCES

1. Allen, P. A., & Allen, J. A. (2013). Basin Analysis Principles and applications to Petroleum Systems (3rd ed.). Wiley Blackwell.

2. Athy, L. F. (1930). Density, Porosity, and Compaction of Sedimentary Rocks. AAPG Bulletin, 14. https://doi.org/10.1306/3D93289E-16B1-11D7-8645000102C1865D

3. Barker, C. E., & Pawlewicz, M. J. (1994). Calculation of vitrinite reflectance from thermal histories and peak temperatures – a comparison of methods. Vitrinite Reflectance as a Maturity Parameter, 14.

4. Bishop, M. (1999). Total petroleum systems of the northwest shelf, Australia: the dingo-m=Mungaroo/barrow and the Locker-Mungaroo/barrow (open-file report) [open-file report].

5. Bray, R. J., Green, P. F., & Duddy, I. R. (1992). Thermal history reconstruction using apatite fission track analysis and vitrinite reflectance: A case study from the UK East Midlands and Southern North Sea. Geological Society, London, Special Publications, 67(1), 3–25. https://doi.org/10.1144/GSL.SP.1992.067.01.01

6. Brodie, J., & White, N. (1994). Sedimentary basin inversion caused by igneous underplating: Northwest European continental shelf. Geology, 22(2), 147. https://doi.org/10.1130/0091-7613(1994)022<0147:SBICBI>2.3.CO;2

7. Burnham, A. K. (2019). Kinetic models of vitrinite, kerogen, and bitumen reflectance. Organic Geochemistry, 131, 50–59. https://doi.org/10.1016/j.orggeochem.2019.03.007

8. Curtis, M., Holford, S., Bunch, M., & Schofield, N. (2019). The spatial distribution of igneous intrusions in the Exmouth Plateau and Exmouth Sub Basin, North West Shelf, Western Australia. ASEG Extended Abstracts, 2019(1), 1–5. https://doi.org/10.1080/22020586.2019.12072966

9. Duddy, I. R., Green, P. F., Gibson, H. J., & Hegarty, K. A. (2004). Regional palaeo-thermal episodes in northern Australia. 25.

10. Holford, S. P., & Schofield, N. (2013). Impacts of Igneous Intrusions on Source and Reservoir Potential in Prospective Sedimentary Basins Along the Western Australian Continental Margin. 13.

11. Johnson, L. M., Rezaee, R., Kadkhodaie, A., Smith, G., & Yu, H. (2017). A new approach for estimating the amount of eroded sediments, a case study from the Canning Basin, Western Australia. Journal of Petroleum Science and Engineering, 156, 19–28. https://doi.org/10.1016/j.petrol.2017.05.008

12. Longley, L., Buessenschuett, L., Clydsdale, L., Cubitt, C., Davis, R., Johnson, M., Marshall, N., Somerville, R., & Spry, T. (2002). The North West Shelf of Australiaea Woodside perspective, The Sedimentary Basins of Western Australia 3: Proceedings of the Petroleum Exploration Society of Australia Symposium. PESA, 27–88.

13. Lü, Z.-X., Ye, S.-J., Yang, X., Li, R., & Qing, Y.-H. (2015). Quantification and timing of porosity evolution in tight sand gas reservoirs: An example from the Middle Jurassic Shaximiao Formation, western Sichuan, China. Petroleum Science, 12(2), 207–217. https://doi.org/10.1007/s12182-015-0021-1

14. Magara, K. (1980). Comparison of porosity-depth relationships of shale and sandstone. Journal of Petroleum Geology, 3, 175–185. https://doi.org/10.1111/j.1747-5457.1980.tb00981.x

15. McClay, K., Scarselli, N., & Jitmahantakul, S. (2013). Igneous Intrusions in the Carnarvon Basin, NW Shelf, Australia. 21.

16. Poelchau, Harald. S. (1993). Modeling an Exhumed Basin: A Method for Estimating Eroded Overburden. AAPG Bulletin, 77. https://doi.org/10.1306/BDFF842A-1718-11D7-8645000102C1865D

17. Ruge, S. M., Scarselli, N., & Bilal, A. (2021). 3D seismic classification of fluid escape pipes in the western Exmouth Plateau, North West Shelf of Australia. Journal of the Geological Society, 178(3). https://doi.org/10.1144/jgs2020-096

18. Rohrman, M. (2015). Delineating the Exmouth mantle plume (NW Australia) from denudation and magmatic addition estimates. Lithosphere, 7(5), 589–600. https://doi.org/10.1130/L445.1

19. Saunders, A. D., Jones, S. M., Morgan, L. A., Pierce, K. L., Widdowson, M., & Xu, Y. G. (2007). Regional uplift associated with continental large igneous provinces: The roles of mantle plumes and the lithosphere. Chemical Geology, 241(3–4), 282–318. https://doi.org/10.1016/j.chemgeo.2007.01.017

20. Sclater, J. G., & Christie, P. A. F. (1980). Continental stretching: An explanation of the Post-Mid-Cretaceous subsidence of the central North Sea Basin. Journal of Geophysical Research: Solid Earth, 85(B7), 3711–3739. https://doi.org/10.1029/JB085iB07p03711

21. Surdam, R. C., Boese, S. W., & Crossey, L. J. (1984). The Chemistry of Secondary Porosity. 24.

22. Tassone, D. R., Holford, S. P., Stoker, M. S., Green, P., Johnson, H., Underhill, J. R., & Hillis, R. R. (2014). Constraining Cenozoic exhumation in the Faroe-Shetland region using sonic transit time data. Basin Research, 26(1), 38–72. https://doi.org/10.1111/bre.12052

23. Velayatham, T., Holford, S. P., & Bunch, M. A. (2018). Ancient fluid flow recorded by remarkably long, buried pockmark trains observed in 3D seismic data, Exmouth Plateau, Northern Carnarvon Basin. Marine and Petroleum Geology, 95, 303–313. https://doi.org/10.1016/j.marpetgeo.2018.05.007

24. Wessel, P., Luis, J. F., Uieda, L., Scharroo, R., Wobbe, F., Smith, W. H. F., & Tian, D. (2019). The Generic Mapping Tools Version 6. Geochemistry, Geophysics, Geosystems, 20(11), 5556–5564. https://doi.org/10.1029/2019GC008515

25. Wessel, Paul, Smith, W. H. F., Scharroo, R., Luis, J., & Wobbe, F. (2013). Generic Mapping Tools: Improved Version Released. Eos, Transactions American Geophysical Union, 94(45), 409–410. https://doi.org/10.1002/2013EO450001

26. White, R., & McKenzie, D. (1989). Magmatism at rift zones: The generation of volcanic continental margins and flood basalts. Journal of Geophysical Research, 94(B6), 7685. https://doi.org/10.1029/JB094iB06p07685

27. Wilkinson, M., & Haszeldine, R. S. (2011). Oil charge preserves exceptional porosity in deeply buried, overpressured, sandstones: Central North Sea, UK. Journal of the Geological Society, 168(6), 1285–1295. https://doi.org/10.1144/0016-76492011-007

28. Wilkinson, M., Haszeldine, R. S., & Fallick, A. E. (2014). Authigenic illite within northern and central North Sea oilfield sandstones: Evidence for post-growth alteration. Clay Minerals, 49(2), 229–246. https://doi.org/10.1180/claymin.2014.049.2.06
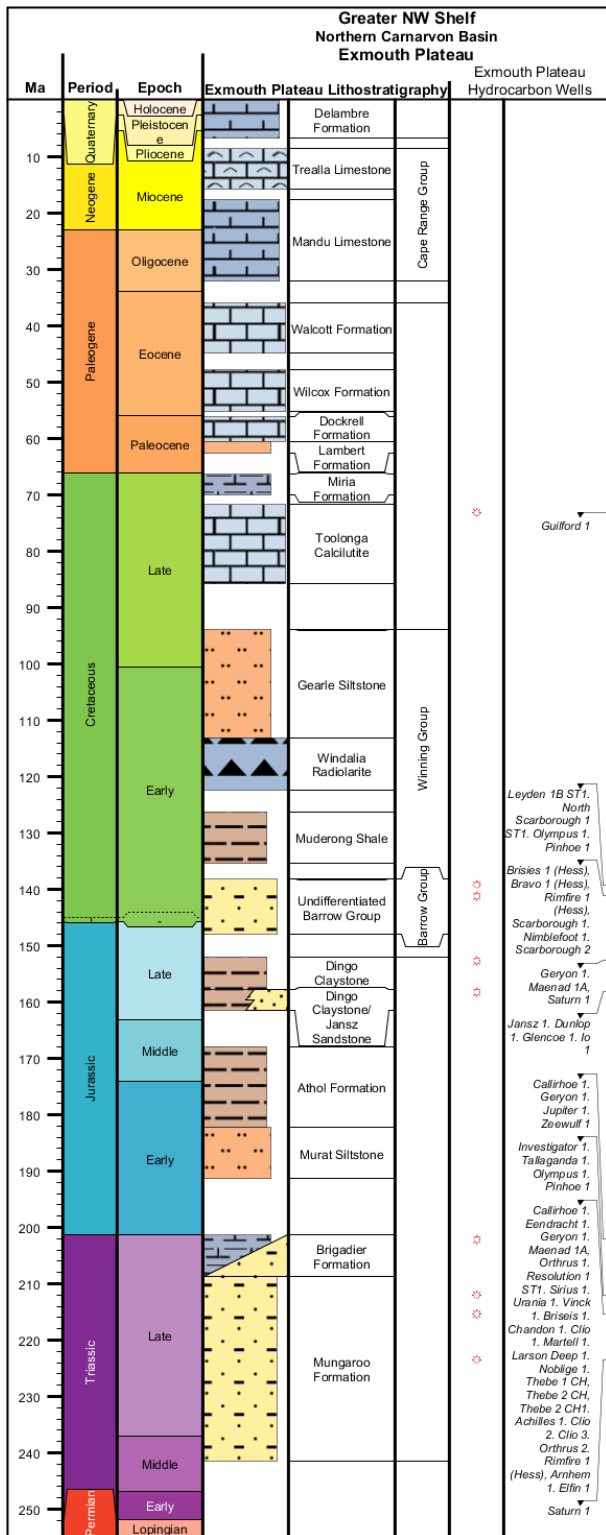
Appendix

Figure 2: The stratigraphic chart of Exmouth Plateau, showing the various lithologies within the study region. The Triassic Mungaroo and Brigadier formations have been used for the uplift modelling. Figure produced with TSCreator Pro 7.4 using the 2016 Australian data pack.
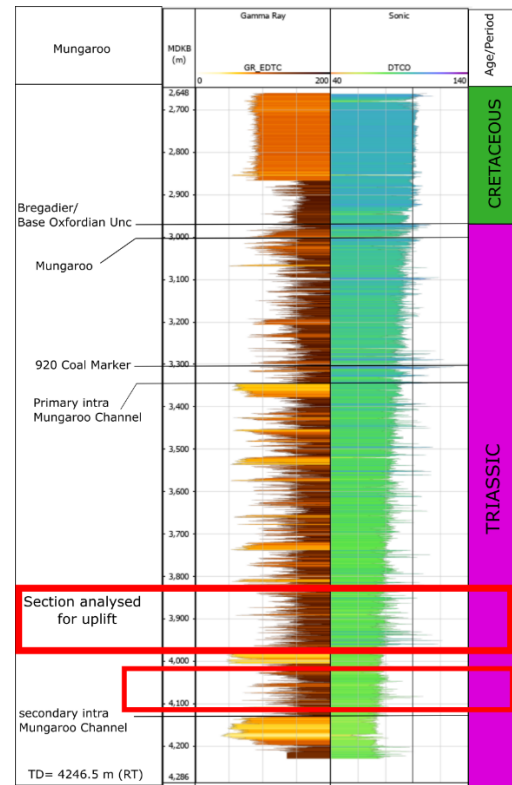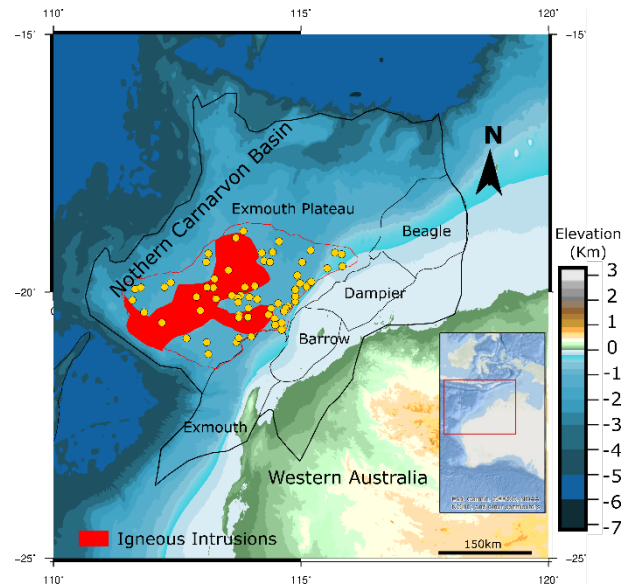

Figure 3: An example of sonic log and Gamma ray log data from Homevale Well (from NOPIMS) used for uplift estimation. Red rectangles show the Triassic shale sections used for uplift estimation on the standard burial curve (Fig. 4).

Table 1: Example of Vitrinite reflectance and porosity-depth data of four well from the study region; see appendix for additional porosity-depth data.

Well	VR (%R)	Depth (m)	Age	dT/dZ °C/km	Q & Depth	Q_0	c
			Vitrinite Reflectance Data		Compaction data		
Sirius	0.42	2855	Jur				
Latitude	0.54	2870	Jur				
-20.8833	0.56	2910	Jur				
Longitude	0.56	3150	Tri		17% @ 3018m	49%	0.27
112.6906	0.62	3215	Tri	33		49%	0.27
	0.64	3270	Tri		16% @ 3240m	49%	0.27
	0.71	3325	Tri		15 % @ 3347	49%	0.27
	0.72	3445	Tri		14% @ 3414m	49%	0.27
	0.85	3470	Tri				
Vinck							
Latitude	0.66	3810	Tri		16% @ 3200m	49%	0.27
-20.5834	0.79	3811	Tri	35	13.9% @ 3799m	49%	0.27
Longitude	0.8	3814	Tri		13.1% @ 3802m	49%	0.27
112.1939					11.0% @ 4461m	49%	0.27
Saturn							
Latitude	0.32	2220	Cen				
-19.9086	0.4	2521	Cret		19% @ 3022m	49%	0.27
Longitude	0.5	3260	Tria		15% @ 3220m	49%	0.27
114.946	0.6	3610	Tria	30	13.5% @ 3500	49%	0.27
	0.68	3710	Tria				
	0.81	3875	Tria				
	0.91	3980	Tria				
Jupiter	0.54	2360	Tria		18% @ 2492m	49%	0.27
Latitude	0.52	2545	Tria				
-19.5802	0.68	2815	Tria				
Longitude	0.72	3050	Tria				
113.5342	0.7	3375	Tria	30	14% @ 3373m	49%	0.27
	1.02	4250	Tria		12% @3866 m	49%	0.27
	1.15	4390	Tria				
	1.4	4750	Tria				
	1.5	4865	Tria				

Figure 7: Topographic map of the Northern Carnarvon Basin (*NOAA NGDC, 2009*) showing the distribution of igneous intrusions (red polygon) and wells used for uplift modelling within the Exmouth Plateau from Curtis et al. (2019). Figure produced using GMT (Wessel et al.,2019).